
Differentially Private Adaptation of Diffusion Models via Noisy Aggregated Embeddings

Anonymous Author(s)

Affiliation

Address

email

Abstract

1 Personalizing large-scale diffusion models poses serious privacy risks, especially
2 when adapting to small, sensitive datasets. A common approach is to fine-tune the
3 model using differentially private stochastic gradient descent (DP-SGD), but this
4 suffers from severe utility degradation due to the high noise needed for privacy,
5 particularly in the small data regime. We propose an alternative that leverages
6 Textual Inversion (TI), which learns an embedding vector for an image or set
7 of images, to enable adaptation under differential privacy (DP) constraints. Our
8 approach, Differentially Private Aggregation via Textual Inversion (DPAgg-TI),
9 adds calibrated noise to the aggregation of per-image embeddings to ensure formal
10 DP guarantees while preserving high output fidelity. We show that DPAgg-TI
11 outperforms DP-SGD finetuning in both utility and robustness under the same
12 privacy budget, achieving results closely matching the non-private baseline on
13 style adaptation tasks using private artwork from a single artist and Paris 2024
14 Olympic pictograms. In contrast, DP-SGD fails to generate meaningful outputs in
15 this setting.

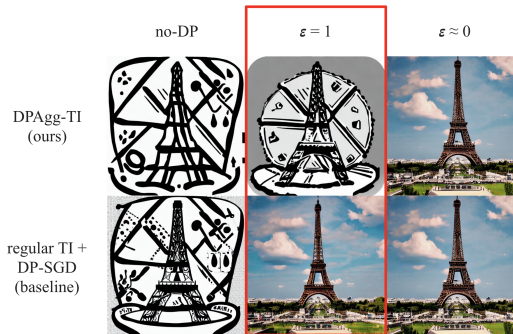


Figure 1: We compare our method (DPAgg-TI, top) to a baseline applying DP-SGD to Textual Inversion (bottom), using the prompt “an icon of the Eiffel Tower in the style of the Paris 2024 Olympic Pictograms.” While the baseline learns a single embedding over the dataset, our method privately aggregates per-image embeddings. At privacy budget $\epsilon = 1$, DPAgg-TI preserves visual fidelity much better than the baseline, and closely matches the non-private output (left), demonstrating a superior privacy-utility tradeoff.

16 1 Introduction

17 The rapid adoption of diffusion models Ho et al. [2020], Song et al. [2021b], Rombach et al. [2022]
18 has raised significant privacy and legal concerns. These models are vulnerable to privacy attacks, such
19 as membership inference Duan et al. [2023], where attackers determine if a specific data point was

20 used for training, and data extraction Carlini et al. [2023], which enables reconstruction of training
 21 data. This risk is amplified during fine-tuning on smaller, domain-specific datasets, where each record
 22 has a greater impact. Additionally, reliance on large datasets scraped without consent raises copyright
 23 concerns Vyas et al. [2023], as diffusion models can reproduce original artworks without credit or
 24 compensation. These issues highlight the urgent need for privacy-preserving technologies and clearer
 25 ethical and legal guidelines for generative models.

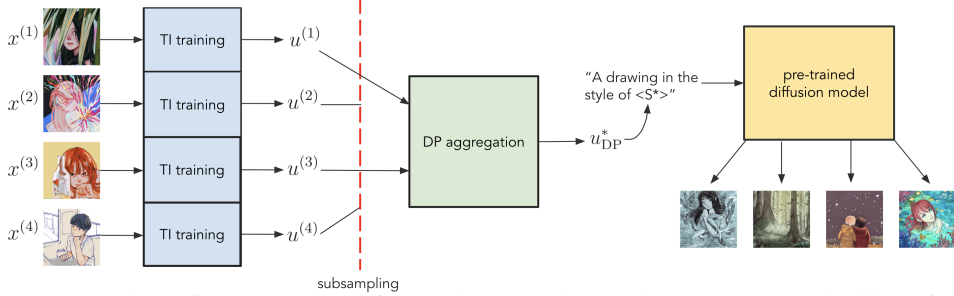


Figure 2: Overview of DPAgg-TI. We first apply Textual Inversion to extract embeddings for each image in the private dataset. These embeddings are then aggregated with differentially private mechanism, incorporating subsampling to produce a private embedding u_{DP}^* . Finally, images are generated using the corresponding token $\langle S^* \rangle$.

26 Differential privacy (DP) Dwork [2006] is a widely adopted framework for addressing these chal-
 27 lenges. One standard approach for ensuring DP in deep learning is Differentially Private Stochastic
 28 Gradient Descent (DP-SGD) Abadi et al. [2016], which modifies traditional SGD by adding noise to
 29 clipped gradients. However, applying DP-SGD to train diffusion models poses several challenges.
 30 It introduces significant computational and memory overhead due to per-sample gradient clipping
 31 Hoory et al. [2021], which is essential for bounding gradient sensitivity Dwork et al. [2006], Abadi
 32 et al. [2016]. DP-SGD is also incompatible with batch-wise operations like batch normalization, as
 33 these link samples and hinder sensitivity analysis. Furthermore, training large models with DP-SGD
 34 often leads to substantial performance degradation, particularly under realistic privacy budgets since
 35 the required noise scales with the gradient norm. Consequently, existing diffusion models trained
 36 with DP-SGD are limited to relatively small-scale images.

37 Independent of privacy concerns, Textual Inversion (TI) Gal et al. [2023] provides an effective method
 38 for adapting diffusion models to specific styles or content without modifying the model. Instead, TI
 39 learns an external embedding vector that captures the style or content of a target image set, which
 40 is then incorporated into text prompts to guide the model’s outputs. A key advantage of TI is its
 41 ability to compress a style into a compact vector, reducing computational and memory demands
 42 while simplifying the application of privacy-preserving mechanisms, as privacy constraints can be
 43 applied directly to embeddings rather than the full model. Additionally, since TI avoids direct model
 44 optimization, it remains efficient and compatible with DP constraints on smaller datasets.

45 In this work, we propose a novel privacy-preserving adaptation method for smaller datasets, lever-
 46 aging TI to avoid the extensive model updates required by DP-SGD. Standard TI does not offer
 47 formal privacy guarantees, so to address this limitation, we introduce a private variant of TI, called
 48 Differentially Private Aggregation via Textual Inversion (DPAgg-TI) and summarize it in Figure 2.
 49 Our method decouples interactions among samples by learning a separate embedding for each target
 50 image, which are then aggregated into a noisy centroid. This approach ensures efficient and secure
 51 adaptation to private datasets.

52 Our experiments demonstrate the effectiveness of DPAgg-TI, showing that TI remains robust in
 53 preserving stylistic fidelity even under privacy constraints. Applying our method to a private artwork
 54 collection by @eveismynname and Paris 2024 Olympics pictograms Paris 2024, we show that
 55 DPAgg-TI captures nuanced stylistic elements while ensuring privacy. We observe a trade-off
 56 between privacy (controlled by DP parameter ϵ) and image quality: lower ϵ reduces fidelity but
 57 maintains the target style under moderate noise. Subsampling further amplifies privacy by reducing
 58 sensitivity to individual data points, mitigating noise impact on image quality. This framework
 59 enables privacy-preserving adaptation of diffusion models to new styles and domains while protecting
 60 sensitive data.

61 Our contributions can be summarized as follows:

62 (1) We propose DPAgg-TI that ensures privacy by learning separate embeddings for individual images
 63 and aggregating them into a noisy centroid.

64 (2) Our approach enables style adaptation without extensive model updates, reducing computational
 65 overhead while preserving privacy.

66 (3) We analyze the trade-off between privacy and image quality, showing that moderate noise
 67 maintains stylistic fidelity while protecting sensitive data.

68 (4) We validate our method on diverse datasets, demonstrating its effectiveness in capturing stylistic
 69 elements under privacy constraints.

70 2 Background and Related Work

71 2.1 Diffusion Models

72 Diffusion models Ho et al. [2020], Song et al. [2021b,a], Rombach et al. [2022] leverage an iterative
 73 denoising process to generate high-quality images that align with a given conditional input from
 74 random noise. In text-to-image generation, this conditional input is based on a textual description (a
 75 prompt) that guides the model in shaping the image to reflect the content and style specified by the
 76 text. To convert the text prompt into a suitable conditional format, it is first broken down into discrete
 77 tokens, each representing a word or sub-word unit. These tokens are then converted into a sequence
 78 of embedding vectors v_i that encapsulate the meaning of each token within the model’s semantic
 79 space. Next, these embeddings pass through a transformer text encoder, such as CLIP Radford et al.
 80 [2021], outputting a single text-conditional vector y that serves as the conditioning input. This vector
 81 y is then incorporated at each denoising step, guiding the model to align the output image with the
 82 specific details outlined in the prompt.

83 The image generation process, also known as the reverse diffusion process, comprises of T discrete
 84 timesteps and starts with pure Gaussian noise x_T . At each decreasing timestep t , the denoising model,
 85 which often utilizes a U-Net structure with cross-attention layers, takes a noisy image x_t and text
 86 conditioning y as inputs and predicts the noise component $\epsilon_\theta(x_t, y, t)$, where θ denotes the denoising
 87 model’s parameters. The predicted noise is then used to make a reverse diffusion step from x_t to
 88 x_{t-1} , iteratively refining the noisy image closer to a coherent output x_0 that aligns with the text
 89 conditional y .

90 The objective function for a text-conditioned diffusion model, given both the noisy image x_t and
 91 the text conditioning y , is typically a mean squared error (MSE) between the true noise ϵ and the
 92 predicted noise $\epsilon_\theta(x_t, y, t)$. The denoising model is therefore trained over:

$$\theta^* = \arg \min_{\theta} \mathbb{E}_{x, \epsilon \sim \mathcal{N}(0, I), t \sim [T]} [\|\epsilon - \epsilon_\theta(x_t, y, t)\|^2]. \quad (1)$$

93 2.2 Textual Inversion.

94 Textual Inversion (TI) Gal et al. [2023] is an adaptation technique that enables personalization using a
 95 small dataset of typically 3-5 images. This approach essentially learns a new token that encapsulates
 96 the semantic meaning of the training images, allowing the model to associate specific visual features
 97 with a custom token.

98 To achieve this, TI trains a new token embedding, denoted as u , representing a placeholder token,
 99 denoted as S . During training, images are conditioned on phrases such as “A photo of S ” or “A
 100 painting in the style of S ”. However, unlike the fixed embeddings of typical tokens v_i , u is a learnable
 101 parameter. Let y_u denote the text conditioning vector resulting from a prompt containing the token S .
 102 Through gradient descent, TI minimizes the diffusion model loss given in (1) with respect to u , while
 103 keeping the diffusion model parameters θ fixed, iteratively refining this embedding to capture the
 104 unique characteristics of the training images. The resulting optimal embedding u^* is formalized as:

$$u^* = \arg \min_u \mathbb{E}_{x, \epsilon \sim \mathcal{N}(0, I), t \sim [T]} [\|\epsilon - \epsilon_\theta(x_t, y_u, t)\|^2]. \quad (2)$$

105 Hence, u^* represents an optimized placeholder token S^* , which can be employed in prompts such as “A
 106 photo of S^* floating in space” or “A drawing of a capybara in the style of S^* ”, enabling the generation
 107 of personalized images that reflect the learned visual characteristics.

108 **2.3 Differential Privacy.**

109 In this work, we adopt differential privacy (DP) Dwork et al. [2006], Dwork [2006] as our privacy
110 framework. Over the past decade, DP has become the gold standard for privacy protection in both
111 research and industry. It measures the stability of a randomized algorithm with respect to changes in
112 an input instance, thereby quantifying the extent to which an adversary can infer the existence of a
113 specific input based on the algorithm’s output.

Definition 1 ((Approximate) Differential Privacy). *For $\varepsilon, \delta \geq 0$, a randomized mechanism $\mathcal{M} : \mathcal{X}^n \rightarrow \mathcal{Y}$ satisfies (ε, δ) -DP if for all neighboring datasets $\mathcal{D}, \mathcal{D}' \in \mathcal{X}^n$ which differ in a single record (i.e., $\|\mathcal{D} - \mathcal{D}'\|_H \leq 1$ where $\|\cdot\|_H$ is the Hamming distance) and all measurable \mathcal{S} in the range of \mathcal{M} , we have that*

$$\mathbb{P}(\mathcal{M}(\mathcal{D}) \in \mathcal{S}) \leq e^\varepsilon \mathbb{P}(\mathcal{M}(\mathcal{D}') \in \mathcal{S}) + \delta.$$

114 When $\delta = 0$, we say \mathcal{M} satisfies ε -pure DP or $(\varepsilon$ -DP).

115 To achieve DP, the Gaussian mechanism is often applied Dwork et al. [2014], Balle and Wang [2018],
116 adding Gaussian noise scaled by the sensitivity of the function f and privacy parameters ε and δ .

117 Specifically, noise with standard deviation $\sigma = \frac{\Delta_f \sqrt{2 \ln(1.25/\delta)}}{\varepsilon}$ is added to the output¹ Balle and
118 Wang [2018], where Δ_f represents ℓ_2 -sensitivity of the target function $f(\cdot)$. When the context is
119 clear, we may omit the subscript f . This mechanism enables a smooth privacy-utility tradeoff and is
120 widely used in privacy-preserving machine learning, including in DP-SGD Abadi et al. [2016], which
121 applies Gaussian noise during model updates to achieve DP.

122 **Privacy Amplification by Subsampling.** Subsampling is a standard technique in DP, where a
123 full dataset of size n is first subsampled to m records without replacement (typically with $m \ll n$)
124 before the privatization mechanism (such as the Gaussian mechanism) is applied. Specifically, if
125 a mechanism provides (ε, δ) -DP on a dataset of size m , it achieves (ε', δ') -DP on the subsampled
126 dataset, where $\delta' = \frac{m}{n} \delta$ and

$$\varepsilon' = \log \left(1 + \frac{m}{n} (e^\varepsilon - 1) \right) = O \left(\frac{m}{n} \varepsilon \right). \quad (3)$$

127 This result is well-known (Steinke [2022, Theorem 29]), with tighter amplification bounds available
128 for Gaussian mechanisms Mironov [2017].

129 **2.4 Private Adaptation of Diffusion Models**

130 Recent advancements in applying DP to diffusion models have aimed to balance privacy preservation
131 with the high utility of generative outputs. Dockhorn et al. Dockhorn et al. [2023] proposed a
132 Differentially Private Diffusion Model (DPDM) that enables privacy-preserving generation of realistic
133 samples, setting a foundational approach for adapting diffusion processes using DP-SGD. Another
134 common strategy involves training a model on a large public dataset, followed by differentially private
135 fine-tuning on a private dataset, as explored by Ghalebikesabi et al. [2023]. While effective in certain
136 contexts, this approach raises privacy concerns, particularly around risks of information leakage
137 during the fine-tuning phase Tramèr et al. [2024].

138 In response to these limitations, various adaptation techniques have emerged. Although not spe-
139 cific to diffusion models, some methods focus on training models on synthetic data followed by
140 DP-constrained fine-tuning, as in the VIP approach Yu et al. [2024], which demonstrates the fea-
141 sibility of applying DP in later adaptation stages. Other approaches explore differentially private
142 learning of feature representations Sander et al. [2024], aiming to distill private information into
143 a generalized embedding space while maintaining DP guarantees. Although these adaptations are
144 not yet implemented for diffusion models, they lay essential groundwork for developing secure and
145 efficient privacy-preserving generative models.

146 **3 Differentially Private Adaptation via Textual Inversion**

147 Let $x^{(1)}, \dots, x^{(n)}$ represent a target dataset of images whose characteristics we wish to privately
148 adapt our image generation towards. Instead of training a single token embedding on the entire

¹In practice, we use numerical privacy accountant such as Balle and Wang [2018], Mironov [2017] to calibrate the noise.

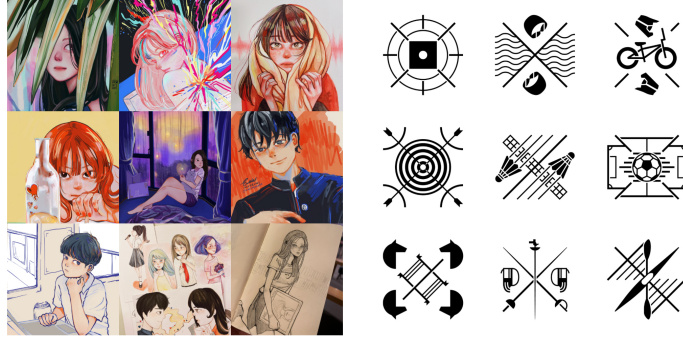


Figure 3: Samples of images used in our style adaptation experiments. **Left:** artwork by @eveismyname ($n = 158$). **Right:** Paris 2024 Olympic pictograms ($n = 47$), © International Olympic Committee, 2023.

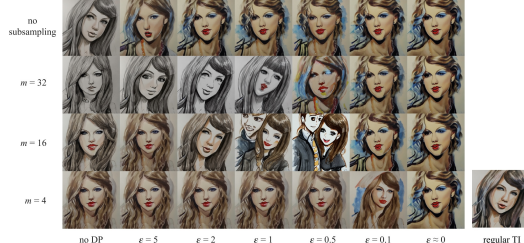


Figure 4: Images generated by Stable Diffusion v1.5 using the prompt “A painting of Taylor Swift in the style of <@eveismyname>”, with the embedding <@eveismyname> trained using different values of m and ϵ .

149 dataset as in regular TI, we train a separate embedding $u^{(i)}$ on each $x^{(i)}$ to obtain a set of embeddings
150 $u^{(1)}, \dots, u^{(n)}$, as illustrated in Figure 2. We can formalize the encoding process as follows:

$$u^{(i)} = \arg \min_u \mathbb{E}_{\epsilon \sim \mathcal{N}(0, I), t} [\|\epsilon - \epsilon_\theta(x_t^{(i)}, y_u, t)\|^2]. \quad (4)$$

151 Then, we can aggregate the embeddings $u^{(1)}, \dots, u^{(n)}$ by calculating the centroid. The purpose of
152 this aggregation is to limit the sensitivity of the final output to each $x^{(i)}$. In order to provide DP
153 guarantees, we also add isotropic Gaussian noise to the centroid. We can therefore define the resulting
154 embedding vector u_{DP}^* as follows:

$$u_{\text{DP}}^* = \frac{1}{n} \sum_{i=1}^n u^{(i)} + \mathcal{N}(0, \sigma^2 I), \quad (5)$$

155 where the minimum σ required to provide (ϵ, δ) -DP is given by the following expression based on
156 Balle and Wang [2018, Theorem 1]:

$$\sigma = \frac{\Delta}{n} \cdot \frac{\sqrt{2 \ln(1.25/\delta)}}{\epsilon}. \quad (6)$$

157 In the context of our problem, $\Delta = \sup_{i,j} \|u^{(i)} - u^{(j)}\|$. Since our embedding vectors are directional,
158 we can normalize each $u^{(i)}$, allowing us to set $\Delta = 2$.

159 The noisy centroid embedding u_{DP}^* can then be used to adapt the downstream image generation
160 process. Similar to regular TI’s u^* , we can use u_{DP}^* to represent a new placeholder token S^* that
161 can be incorporated into prompts for personalized image generation. While u_{DP}^* may not fully solve
162 the TI optimization problem presented in (2), it provides provable privacy guarantees, with only a
163 minimal trade-off in accurately representing the style of the target dataset.

164 To reduce the amount of noise needed to provide the same level of DP, we employ subsampling:
165 instead of computing the centroid over all n embedding vectors, we randomly sample $m \leq n$
166 embedding vectors without replacement and compute the centroid over only the sampled vectors.
167 Then the standard privacy amplification by subsampling bounds (such as (3)) can be applied. Formally,



Figure 5: Images generated by Stable Diffusion v1.5 using the prompt “Icon of a dragon in the style of <Paris 2024 Pictograms>”, with the embedding <Paris 2024 Pictograms> trained using different values of m and ε .

168 we sample $D_{\text{sub}} \subseteq \{u^{(1)}, \dots, u^{(n)}\}$ where $|D_{\text{sub}}| = m$, and compute the output embedding as
169 follows:

$$u_{\text{DP}}^* = \frac{1}{m} \sum_{u^{(i)} \in D_{\text{sub}}} u^{(i)} + \mathcal{N}(0, \sigma^2 I), \quad (7)$$

170 where σ can be computed numerically for any target ε, δ and subsampling rate $\frac{m}{n}$.

171 4 Experimental Results

172 4.1 Datasets

173 We compiled two datasets to evaluate our style adaptation method, specifically selecting content
174 unlikely to be recognized by Stable Diffusion v1.5, our base model.

175 The first dataset consists of 158 artworks by the artist @eveismynname, who has granted consent
176 for non-commercial use. This dataset allows us to assess whether models can capture artistic styles
177 without memorizing individual works. While some of these artworks may have been publicly
178 accessible on social media, making incidental inclusion in Stable Diffusion’s pretraining possible,
179 the artist’s limited recognition and relatively small portfolio reduce the likelihood that the model has
180 internalized her unique style. This dataset serves as a controlled test for privacy-preserving style
181 transfer on individual artistic collections.

182 The second dataset contains 47 pictograms from the Paris 2024 Olympics Paris 2024, permitted
183 strictly for non-commercial editorial use International Olympic Committee. These pictograms were
184 officially released in February 2023, several months after the release of Stable Diffusion v1.5, ensuring
185 they were absent from the model’s pretraining data. This dataset allows us to assess how well our
186 approach adapts to newly introduced visual styles that the base model has never encountered.

187 Both datasets are used to test the ability of our method to extract and transfer stylistic elements while
188 preserving privacy. Representative samples are shown in Figure 3.

189 4.2 Style Transfer Results

190 Using both the @eveismynname and Paris 2024 pictograms dataset, we trained TI Gal et al. [2023]
191 embeddings on Stable Diffusion v1.5 Rombach et al. [2022] using DPAgg-TI. Our primary goal
192 is to investigate how DP configurations, specifically the privacy budget ε and subsampling size m ,
193 affect the generated images quality and privacy resilience. For regular TI, we utilize the default
194 process to embed the private dataset without any additional noise. For the DPAgg-TI, we test multiple
195 configurations of m and ε to analyze the trade-off between image fidelity and privacy.

196 Figures 4 and 5 present generated images across two key configurations: (1) regular TI without
197 DP, (2) DPAgg-TI with DP at different values of m and ε . We used the same random seed to
198 generate embeddings, subsample images, and sample DP noise for ease of visual comparison between
199 different configurations. As with common practice, we set $\delta = 1/n$. Since σ is undefined for

200 $\varepsilon = 0$, we demonstrate the results of $\varepsilon \approx 0$, in other words, infinite noise, by setting $\varepsilon = 10^{-5}$.
201 The purpose of this parameter value is to demonstrate the image generated when u_{DP}^* contains zero
202 information about the target dataset. Images generated without DP closely resemble the unique
203 stylistic elements of the target dataset. In particular, images adapted using `@eveismyname` images
204 displayed crisp details and nuanced color gradients characteristic of the artist’s work, while those of
205 Paris 2024 pictograms captured the logo’s original structure. In contrast, DP configurations introduce
206 a discernible degradation in image quality, with lower epsilon values and smaller subsampling sizes
207 resulting in diminished stylistic fidelity.

208 As $\varepsilon \rightarrow 0$, the resulting token embedding u_{DP}^* gradually loses its semantic meaning, leading to a
209 loss of stylistic fidelity. In particular, $y_{u_{\text{DP}}^*}$ tends towards y (a conditioning vector independent of
210 the learnable embedding). In our results, this manifests as a painting of Taylor Swift devoid of the
211 artist-specific stylistic elements, or a generic icon of a dragon (with color, as opposed to the black
212 and white design of the pictograms). With this in mind, ε can be interpreted as a drift parameter,
213 representing the progression from the optimal u_{DP}^* towards infinity, gradually steering the generated
214 image away from the target style in exchange for stronger privacy guarantees. We also observe
215 instances where there is a temporary drop in prompt fidelity (e.g., $m = 16, \varepsilon \in [0.5, 1]$ in Figure 4
216 and intermediate ε values in Figure 5) which restores as u_{DP}^* drifts even further from its optimal value.
217 We hypothesize that this is due to drifted u_{DP}^* capturing a different meaning unrelated to the prompt,
218 before losing any meaning that could be interpreted by Stable Diffusion’s text encoder, causing u_{DP}^*
219 to be disregarded from $y_{u_{\text{DP}}^*}$ and the prompt fidelity to be restored. Another possible explanation is
220 that the temporary drop in prompt fidelity is due to the drift path of u_{DP}^* passing through non-linear
221 regions within embedding space. We leave further investigations into this observation for future work.

222 Meanwhile, reducing m also reduces the sensitivity of the generated image to ε , as evident by the
223 observation that, on both datasets at $m = 4$, (subsampling rate below 0.1) image generation can
224 tolerate ε as low as 0.5 without significant changes in visual characteristics, and retaining stylistic
225 elements of the target dataset at ε as low as 0.1. This strong boost in robustness comes at a small
226 price of base style capture fidelity. As observed in Figures 4 and 5, we can also treat subsampling as
227 an introduction of noise. Mathematically, the subsample centroid is an unbiased estimate of the true
228 centroid, and so the subsampling process itself defines a distribution centered at the true centroid.
229 However, the amount of noise introduced by the subsampling process is limited by the individual
230 image embeddings, as a subsample centroid can only stray from the true centroid as much as the
231 biggest outlier in the dataset.

232 4.3 Quantitative Evaluation

233 **User Study** To evaluate the utility of our approach under different DP and subsampling configura-
234 tions, we conducted a user study with 25 participants. Each participant was shown reference images
235 from the target dataset and asked to compare pairs of generated images, selecting the one that better
236 captured the style of the reference images. Images were generated using 10 prompts and adapted
237 TI embeddings for the `@eveismyname` and Paris 2024 Pictogram datasets, resulting in 20 groups
238 of images. Each participant evaluated two groups, one randomly selected from each dataset, with
239 comparisons focusing on model configurations differing by DP noise and subsampling size.

240 Survey results, summarized in Table 1 in Appendix A, align with our design goals. Participants
241 showed no clear preference between regular TI and DPAgg-TI, suggesting that our privacy-preserving
242 approach maintains perceptual quality. As expected, both DP noise and reduced subsampling size
243 degraded style fidelity, consistent with the trade-offs inherent in differential privacy. Preferences at
244 $\varepsilon = 1$ were split, but subsampling was generally favored, reinforcing its role in reducing noise impact
245 while preserving style.

246 **Kernel Inception Distance** The Kernel Inception Distance (KID) Bińkowski et al. [2018] is a
247 metric for evaluating generative models by measuring the difference between the distributions of
248 generated and training images in an embedding space. To compute KID, images generated by the
249 model and real training images are passed through an Inception network Szegedy et al. [2015], and
250 their distributional differences are estimated. Unlike the more commonly used Fréchet Inception
251 Distance (FID) Heusel et al. [2017], KID is an unbiased estimator of the true divergence between the
252 learned and target distributions Jayasumana et al. [2024], making it more suitable for smaller datasets,
253 as in our case.

254 We report KID scores for different parameters in Tables 2 and 3 (see Appendix B), showing that
 255 DPAgg-TI maintains the style transfer fidelity of TI while ensuring differential privacy. Further
 256 discussion of these results is also provided in Appendix B.

257 **Ablation Study: Textual Inversion with DP-SGD** A natural question that arises is how well
 258 our approach compares to the naive method of applying DP-SGD to regular TI training. We there-
 259 fore integrated DP-SGD into the TI codebase using the Opacus library and trained similar embed-
 260 dings on the @eveismynname and Paris 2024 datasets. We found that in most cases, notably the
 261 @eveismynname dataset, the amount of noise required for DP-SGD to achieve a reasonable value of
 262 ϵ for DP is so high that the resulting embedding contains negligible information about the training
 263 dataset. In particular, the results for $\epsilon = 1$ are almost indistinguishable to $\epsilon \approx 0$, as shown in Figure
 264 6. We believe that this is simply because DP-SGD is not designed to handle such small datasets in
 265 the order of 100 images. Additional results can be found in Appendix F.

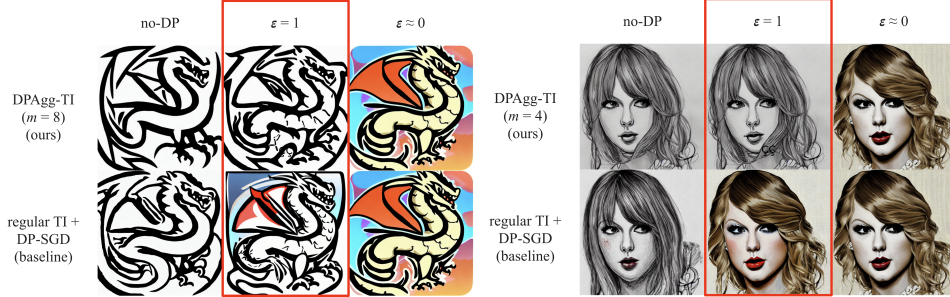


Figure 6: Comparing our approach to applying DP-SGD to regular TI using prompts “an icon of a dragon in the style of the Paris 2024 Olympic Pictograms” and “a painting of Taylor Swift in the style of @eveismynname” respectively. Note that our method aggregates individual TI embeddings for each training image, whereas the baseline trains a single TI embedding over the entire dataset.

266 5 Copyright Protection Implications

267 Our proposed mechanism can also be interpreted through the lens of *copyright protection*. This
 268 connection is grounded in the framework of *Near Access-Freeness* (NAF) [Vyas et al., 2023], which
 269 evaluates whether a model’s outputs reveal undue influence from specific data points by comparing
 270 them to those from a safe model trained without access to the same data. Since DPAgg-TI satisfies
 271 ϵ -DP, it also satisfies ϵ -NAF, which means the adapted model behaves similarly to one that never
 272 saw the private images, under the NAF criterion. However, we emphasize that this guarantee holds
 273 only within the NAF framework; it does not constitute a general claim about content similarity or
 274 legal compliance. Crucially, DPAgg-TI is designed to adapt to the *style* of private images, not their
 275 specific content. Prior work and legal precedent suggest that style imitation is generally considered
 276 *fair use* and does not constitute infringement [Vyas et al., 2023]. Thus, our mechanism aligns with the
 277 intended protections of NAF: it avoids memorization while still enabling meaningful personalization
 278 and stylistic adaptation. We defer the details of copyright protection to Appendix D.

279 6 Conclusion

280 We presented a differentially private adaptation method for diffusion models based on Textual
 281 Inversion, enabling privacy-preserving style transfer without the need for full model fine-tuning. By
 282 learning per-image embeddings and aggregating them with calibrated noise, our method, DPAgg-TI,
 283 achieves strong formal privacy guarantees while maintaining high output fidelity. Experiments
 284 on private artwork and Paris 2024 pictograms show that DPAgg-TI consistently outperforms DP-
 285 SGD, which fails to produce meaningful results under comparable privacy budgets. These results
 286 highlight the effectiveness of embedding-level adaptation as an efficient and scalable alternative
 287 to traditional gradient-based approaches, especially in low-data regimes. Unlike DP-SGD, which
 288 introduces significant computational overhead and utility degradation, DPAgg-TI is lightweight,
 289 modular, and compatible with existing diffusion backbones. Our findings suggest that embedding-
 290 centric approaches offer a promising direction for privacy-aware personalization, and motivate further
 291 research into cross-modal extensions, improved aggregation techniques, and integration with broader
 292 privacy-preserving frameworks.

293 **References**

294 M. Abadi, A. Chu, I. Goodfellow, H. B. McMahan, I. Mironov, K. Talwar, and L. Zhang. Deep
295 learning with differential privacy. In *ACM SIGSAC*, 2016.

296 B. Balle and Y.-X. Wang. Improving the gaussian mechanism for differential privacy: Analytical
297 calibration and optimal denoising. In *ICML*, 2018.

298 A. Bansal, H.-M. Chu, A. Schwarzschild, S. Sengupta, M. Goldblum, J. Geiping, and T. Goldstein.
299 Universal guidance for diffusion models. In *ICLR*, 2024.

300 M. Bińkowski, D. J. Sutherland, M. Arbel, and A. Gretton. Demystifying mmd gans, 2018.

301 N. Carlini, J. Hayes, M. Nasr, M. Jagielski, V. Sehwag, F. Tramer, B. Balle, D. Ippolito, and E. Wallace.
302 Extracting training data from diffusion models. In *USENIX Security*, 2023.

303 T. Dockhorn, T. Cao, A. Vahdat, and K. Kreis. Differentially private diffusion models. *TMLR*, 2023.

304 J. Duan, F. Kong, S. Wang, X. Shi, and K. Xu. Are diffusion models vulnerable to membership
305 inference attacks? In *ICML*, 2023.

306 C. Dwork. Differential privacy. In *ICALP*, 2006.

307 C. Dwork, F. McSherry, K. Nissim, and A. Smith. Calibrating noise to sensitivity in private data
308 analysis. In *TCC*, 2006.

309 C. Dwork, A. Roth, et al. The algorithmic foundations of differential privacy. *Foundations and
310 Trends® in Theoretical Computer Science*, 9(3–4):211–407, 2014.

311 N. Elkin-Koren, U. Hacohen, R. Livni, and S. Moran. Can copyright be reduced to privacy? *arXiv
312 preprint arXiv:2305.14822*, 2023.

313 R. Gal, Y. Alaluf, Y. Atzmon, O. Patashnik, A. H. Bermano, G. Chechik, and D. Cohen-or. An image
314 is worth one word: Personalizing text-to-image generation using textual inversion. In *ICLR*, 2023.

315 S. Ghalebikesabi, L. Berrada, S. Gowal, I. Ktena, R. Stanforth, J. Hayes, S. De, S. L. Smith, O. Wiles,
316 and B. Balle. Differentially private diffusion models generate useful synthetic images. *arXiv
317 preprint arXiv:2302.13861*, 2023.

318 M. Heusel, H. Ramsauer, T. Unterthiner, B. Nessler, and S. Hochreiter. Gans trained by a two
319 time-scale update rule converge to a local nash equilibrium. In I. Guyon, U. V. Luxburg, S. Bengio,
320 H. Wallach, R. Fergus, S. Vishwanathan, and R. Garnett, editors, *Advances in Neural Information
321 Processing Systems*, volume 30. Curran Associates, Inc., 2017. URL https://proceedings.neurips.cc/paper_files/paper/2017/file/8a1d694707eb0fefe65871369074926d-Paper.pdf.

323 J. Ho, A. Jain, and P. Abbeel. Denoising diffusion probabilistic models. *NeurIPS*, 2020.

324 S. Hoory, A. Feder, A. Tendler, S. Erell, A. Peled-Cohen, I. Laish, H. Nakhost, U. Stemmer,
325 A. Benjamini, A. Hassidim, et al. Learning and evaluating a differentially private pre-trained
326 language model. In *Findings of the Association for Computational Linguistics: EMNLP 2021*,
327 pages 1178–1189, 2021.

328 Innat. Van gogh paintings. <https://www.kaggle.com/datasets/ipythonx/van-gogh-paintings>.

329 International Olympic Committee. Olympic properties. <https://olympics.com/ioc/olympic-properties>.

330 S. Jayasumana, S. Ramalingam, A. Veit, D. Glasner, A. Chakrabarti, and S. Kumar. Rethinking
331 fid: Towards a better evaluation metric for image generation. In *2024 IEEE/CVF Conference
332 on Computer Vision and Pattern Recognition (CVPR)*, page 9307–9315. IEEE, June 2024. doi:
333 10.1109/cvpr52733.2024.00889. URL <http://dx.doi.org/10.1109/CVPR52733.2024.00889>.

334 I. Mironov. Rényi differential privacy. In *CSF*, 2017.

335 Paris 2024. Paris 2024 - pictograms. <https://olympics.com/en/paris-2024/the-games/the-brand/pictograms>.

337 A. Radford, J. W. Kim, C. Hallacy, A. Ramesh, G. Goh, S. Agarwal, G. Sastry, A. Askell, P. Mishkin,
338 J. Clark, et al. Learning transferable visual models from natural language supervision. In *ICML*,
339 2021.

340 R. Rombach, A. Blattmann, D. Lorenz, P. Esser, and B. Ommer. High-resolution image synthesis
341 with latent diffusion models. In *CVPR*, 2022.

342 T. Sander, Y. Yu, M. Sanjabi, A. O. Durmus, Y. Ma, K. Chaudhuri, and C. Guo. Differentially private
343 representation learning via image captioning. In *ICML*, 2024.

344 J. Song, C. Meng, and S. Ermon. Denoising diffusion implicit models. In *ICLR*, 2021a.

345 Y. Song, J. Sohl-Dickstein, D. P. Kingma, A. Kumar, S. Ermon, and B. Poole. Score-based generative
346 modeling through stochastic differential equations. In *ICLR*, 2021b.

347 T. Steinke. Composition of differential privacy & privacy amplification by subsampling. *arXiv
348 preprint arXiv:2210.00597*, 2022.

349 C. Szegedy, V. Vanhoucke, S. Ioffe, J. Shlens, and Z. Wojna. Rethinking the inception architecture
350 for computer vision, 2015. URL <https://arxiv.org/abs/1512.00567>.

351 F. Tramèr, G. Kamath, and N. Carlini. Position: Considerations for differentially private learning
352 with large-scale public pretraining. In *ICML*, 2024.

353 N. Vyas, S. M. Kakade, and B. Barak. On provable copyright protection for generative models. In
354 *ICML*, 2023.

355 Y. Yu, M. Sanjabi, Y. Ma, K. Chaudhuri, and C. Guo. Vip: A differentially private foundation model
356 for computer vision. In *ICML*, 2024.

357 **A User Study**

	regular TI	No Adaptation	Unsure
<i>@eveismyname</i>	19	4	2
<i>Paris 2024</i>	16	6	3
	DPAgg-TI (no DP, no subsampling)	No Adaptation	Unsure
<i>@eveismyname</i>	16	9	0
<i>Paris 2024</i>	15	4	6
	regular TI	DPAgg-TI (no DP, no subsamp.)	Unsure
<i>@eveismyname</i>	12	13	0
<i>Paris 2024</i>	9	10	6
	regular TI	DPAgg-TI (no DP, subsamp. $m = 8$)	Unsure
<i>@eveismyname</i>	16	6	3
<i>Paris 2024</i>	7	13	5
	DPAgg-TI (no DP, no subsampling)	DPAgg-TI (no DP, subsamp. $m = 8$)	Unsure
<i>@eveismyname</i>	18	4	3
<i>Paris 2024</i>	10	8	7
	DPAgg-TI ($\varepsilon = 1$) no subsampling	DPAgg-TI ($\varepsilon = 1$, subsamp. $m = 8$)	Unsure
<i>@eveismyname</i>	14	10	1
<i>Paris 2024</i>	3	16	6
	DPAgg-TI (no DP, no subsampling)	Style Guidance	Unsure
<i>@eveismyname</i>	16	8	1
<i>Paris 2024</i>	20	2	3
	DPAgg-TI ($\varepsilon = 1$, subsamp. $m = 8$)	Style Guidance	Unsure
<i>@eveismyname</i>	16	8	1
<i>Paris 2024</i>	19	2	4
	DPAgg-TI (no DP, subsamp. $m = 8$)	DPAgg-TI ($\varepsilon = 1$, subsamp. $m = 8$)	Unsure
<i>@eveismyname</i>	8	5	12
<i>Paris 2024</i>	15	4	6

Table 1: Survey Results.

358 **A.1 Study Design and Objective**

359 The user study aimed to assess the utility of our approach under different DP and subsampling
 360 configurations by evaluating the models' ability to adapt to novel styles. The study involved 25
 361 participants, each of whom was tasked with comparing images generated using various configurations
 362 and selecting the one that better captured the style of reference images.

363 **A.2 Experimental Setup**

364 Participants were shown reference images from two datasets:

365 • The *@eveismyname* dataset of private artwork.

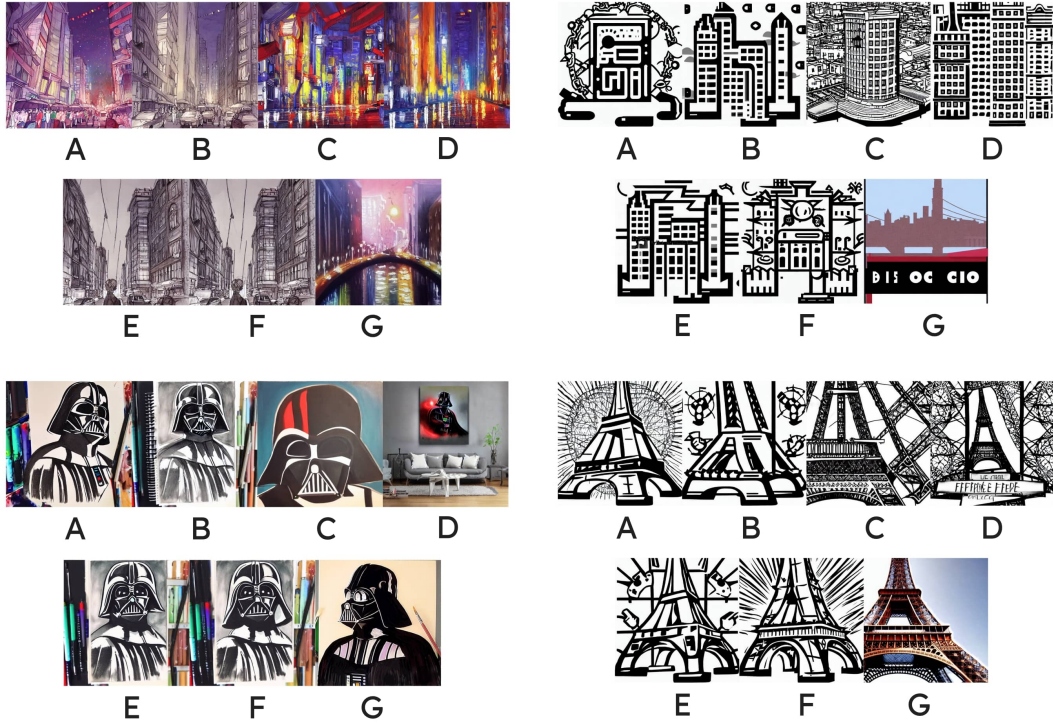


Figure 7: Samples of image sets used in our user study. Participants are asked to compare 2 images at a time.

366 • The Paris 2024 Pictogram dataset.

367 For each dataset, 10 prompts were used to generate images, resulting in 20 groups of images (10
 368 prompts per dataset). Each group included images generated using the same prompt and dataset but
 369 with different model configurations. Configurations varied in the addition of DP noise and the size of
 370 subsampling.

371 • Original Textual Inversion (TI)
 372 • DPAgg-TI ($\varepsilon = \infty$, no DP) w/o subsampling
 373 • DPAgg-TI ($\varepsilon = 1$) without subsampling
 374 • No Adaptation
 375 • DPAgg-TI ($\varepsilon = \infty$, no DP) with subsampling ($m = 8$)
 376 • DPAgg-TI ($\varepsilon = 1$) with subsampling ($m = 8$)
 377 • Style Guidance (SG)

378 **A.3 Survey Procedure**

379 Participants were asked to evaluate two groups of images: one randomly selected from the
 380 @eveismyname dataset and one from the Paris 2024 Pictogram dataset. For each group:

- 381 1. Participants were shown reference images from the target dataset.
- 382 2. They were presented with pairs of images generated using different model configurations
 383 for the same prompt.
- 384 3. Participants selected the image they felt better captured the style of the reference images.

385 **A.4 Evaluation Metrics**

386 The study focused on assessing:

387 • Participants' preference between regular TI and DPAgg-TI for style adaptation.
 388 • The impact of DP noise and subsampling size on the perceived utility of style transfer.

389 **A.5 Results and Analysis**

390 The results are summarized in Table 1. Key observations include:

391 • Participants showed no clear preference between regular TI and DPAgg-TI in capturing
 392 styles for either dataset.
 393 • Both DP noise and reduced subsampling size decreased the perceived quality of style
 394 transfer.
 395 • Preferences were split between configurations with $\varepsilon = 1$ with and without subsampling,
 396 though subsampling generally had favorable outcomes.

397 These findings highlight the trade-off between increased DP robustness and reduced utility, suggesting
 398 that the optimal configuration may depend on subjective preferences and specific application
 399 requirements.

400 **B Kernel Inception Distance**

m	No DP	$\varepsilon = 5.0$	$\varepsilon = 1.0$	$\varepsilon = 0.5$	$\varepsilon = 0.1$	$\varepsilon \approx 0$
–	0.0441 ± 0.0027	0.0798 ± 0.0032	0.0526 ± 0.0022	0.0688 ± 0.0020	0.1114 ± 0.0032	0.0654 ± 0.0027
32	0.0753 ± 0.0047	0.0836 ± 0.0042	0.1166 ± 0.0037	0.0295 ± 0.0019	0.0644 ± 0.0021	0.0650 ± 0.0025
16	0.0350 ± 0.0020	0.0381 ± 0.0018	0.0663 ± 0.0025	0.1303 ± 0.0033	0.0438 ± 0.0030	0.0660 ± 0.0029
8	0.0359 ± 0.0018	0.0364 ± 0.0017	0.0366 ± 0.0019	0.0394 ± 0.0025	0.0527 ± 0.0033	0.0654 ± 0.0024
4	0.0246 ± 0.0013	0.0251 ± 0.0016	0.0249 ± 0.0014	0.0256 ± 0.0012	0.0313 ± 0.0017	0.0653 ± 0.0023
ctrl	0.0314 ± 0.0010	–	–	–	–	–

Table 2: KID scores of DPAgg-TI on `@eveismynname` dataset for various ε values ranging from $\varepsilon = 10^{-5}, 0.1, 0.5, 1.0, 5.0$ (including no DP) under different subsampling levels ($m = 4, 8, 16, 32$) as well as regular TI (ctrl). Reported values are the mean \pm standard deviation over 100 random subsamples.

m	No DP	$\varepsilon = 5.0$	$\varepsilon = 1.0$	$\varepsilon = 0.5$	$\varepsilon = 0.1$	$\varepsilon \approx 0$
–	0.1153 ± 0.0055	0.1194 ± 0.0054	0.1306 ± 0.0046	0.1395 ± 0.0057	0.1201 ± 0.0053	0.1274 ± 0.0055
32	0.1222 ± 0.0066	0.1036 ± 0.0065	0.1375 ± 0.0047	0.1311 ± 0.0048	0.1248 ± 0.0060	0.1258 ± 0.0054
16	0.1321 ± 0.0057	0.1411 ± 0.0077	0.1309 ± 0.0061	0.1380 ± 0.0047	0.1359 ± 0.0060	0.1273 ± 0.0057
8	0.1303 ± 0.0084	0.1303 ± 0.0074	0.1112 ± 0.0062	0.1311 ± 0.0064	0.1318 ± 0.0052	0.1267 ± 0.0056
4	0.1158 ± 0.0057	0.1085 ± 0.0056	0.1184 ± 0.0068	0.1194 ± 0.0065	0.1592 ± 0.0065	0.1268 ± 0.0055
ctrl	0.1383 ± 0.0066	–	–	–	–	–

Table 3: KID scores of DPAgg-TI on Paris dataset for various ε values ranging from $\varepsilon = 1e-5, 0.1, 0.5, 1.0, 5.0$ (including no DP) under different subsampling levels ($m = 4, 8, 16, 32$) as well as regular TI (ctrl). Reported values are the mean \pm standard deviation over 100 random subsamples.

401 Our results indicate that DPAgg-TI preserves the style transfer fidelity of TI while also ensuring
 402 differential privacy. Notably, for `@eveismynname` ($m = 4$) at low privacy budgets, we observe even
 403 lower KID values than standard TI, suggesting enhanced style alignment. Similarly, results for the
 404 Paris 2024 dataset follow a comparable trend, with DPAgg-TI achieving KID scores similar to TI at
 405 low privacy budgets. However, the overall KID scores for this dataset remain high within the context
 406 of diffusion model style transfer.

407 Upon inspecting the generated images (Figure 8), we hypothesize that the abstract and out-of-
 408 distribution nature of the Paris 2024 images poses a challenge for the Inception network, leading to
 409 less meaningful feature embeddings. This likely inflates the measured embedding distances between
 410 generated and reference images, resulting in higher-than-expected KID values.

411 For KID evaluations, we used prompts similar to those employed during TI training: “A painting/icon
 412 in the style of S^* ”. Consistent with the training image captions, these prompts do not specify a
 413 subject. For each parameter configuration, we generate 100 images and compute KID by repeatedly
 414 subsampling the larger of the real and generated sets to match the size of the smaller set, 100 times,
 415 then averaging the resulting KID scores.



Figure 8: Sample of generated images for KID evaluations with respect to the Paris 2024 dataset.

416 C Differentially Private Adaptation via Style Guidance

417 C.1 Background: Denoising Diffusion Implicit Models

418 Denoising Diffusion Implicit Models (DDIM) sampling Song et al. [2021a] uses the predicted noise
 419 $\epsilon_\theta(x_t, y, t)$ and a noise schedule represented by an array of scalars $\{\alpha_t\}_{t=1}^T$ to first predict a clean
 420 image \hat{x}_0 , then makes a small step in the direction of \hat{x}_0 to obtain x_{t-1} . The reverse diffusion process
 421 for DDIM sampling can be formalized as follows:

$$\hat{x}_0 = \frac{x_t - \sqrt{1 - \alpha_t} \epsilon_\theta(x_t, y, t)}{\sqrt{\alpha_t}} \quad (8)$$

$$x_{t-1} = \sqrt{\alpha_{t-1}} \hat{x}_0 + \sqrt{1 - \alpha_{t-1}} \epsilon_\theta(x_t, y, t). \quad (9)$$

423 C.2 Implementation

424 We extend our approach to style guidance (SG) by leveraging the framework of Universal Guidance
 425 Bansal et al. [2024]. Specifically, we focus on CLIP-based style guidance, which optimizes the
 426 similarity between the CLIP embeddings of a target image and the generated image.

427 We encode each target image $x^{(i)}$ as $u^{(i)}$ via a CLIP image encoder, then aggregate the embeddings
 428 $u^{(1)}, \dots, u^{(n)}$ into u_{DP}^* using (5) or (7), depending on whether subsampling is applied. The aggregated
 429 embedding u_{DP}^* is then incorporated into the reverse diffusion process as a style guide.

430 Let x_c denote the target style image, x_t the noisy image at step t , and $\mathcal{E}(\cdot)$ the CLIP image encoder.
 431 The forward guidance process is defined as follows:

$$\hat{\epsilon}_\theta(x_t, y, t) = \epsilon_\theta(x_t, y, t) + w \sqrt{1 - \alpha_t} \nabla_{x_t} \ell_{\text{cos}}(\mathcal{E}(x_t), \mathcal{E}(\hat{x}_0)), \quad (10)$$

432 where w is a guidance weight and ℓ_{cos} is the negative cosine similarity loss. For a detailed description
 433 of Universal Guidance, including the backward guidance process and per-step self-recurrence, we
 434 refer the reader to the original paper. The reverse diffusion step replaces $\epsilon_\theta(x_t, y, t)$ with $\hat{\epsilon}_\theta(x_t, y, t)$,
 435 generating an image x_0 that aligns with the text conditioning y while incorporating the stylistic
 436 characteristics of x_c .

437 To integrate differential privacy, we encode each target image $x^{(i)}$ into $u^{(i)} = \mathcal{E}(x^{(i)})$ and aggregate
 438 these embeddings into u_{DP}^* using the centroid method. The aggregated u_{DP}^* guides the reverse
 439 diffusion process:

$$\hat{\epsilon}_\theta(x_t, y, t) = \epsilon_\theta(x_t, y, t) + w \sqrt{1 - \alpha_t} \nabla_{x_t} \ell_{\text{cos}}(u_{\text{DP}}^*, \mathcal{E}(\hat{x}_0)). \quad (11)$$

440 This ensures privacy-preserving style transfer while maintaining high stylistic fidelity.

441 C.3 Style Transfer Results

442 We apply our SG-based approach to both datasets. While it provides privacy protection by obfuscating
 443 embedding details, the resulting images captured only generalized stylistic elements and lack the
 444 detailed fidelity and coherence achieved with the TI-based method. As shown in Figure 9, this
 445 highlights the superiority of TI in balancing privacy and high-quality image generation.



Figure 9: Attempts of using universal guidance to generate drawings of Taylor Swift and icons of the Eiffel Tower in the styles of @eveismyname and Paris 2024 Pictograms respectively. Here, we apply no subsampling or DP-noise.

446 The reduced effectiveness of SG for style transfer may stem from its sensitivity to hyperparameters
 447 such as the guidance weight w , leading to instability. Although Bansal et al. [2024] proposed
 448 remedies, namely backward guidance and per-step self-recurrence, these proved insufficient for our
 449 application. Additionally, the CLIP embeddings may not retain enough stylistic detail after the
 450 aggregation.

451 **C.4 Ablation**

452 To better understand the limited effectiveness of style guidance in our experiments, despite its success
 453 in Bansal et al. [2024], we applied our approach to a dataset of 143 paintings from Van Gogh’s
 454 Saint-Paul Asylum, Saint-Rémy collectionInnat (Figure 10). Unlike the @eveismyname and Paris
 455 2024 datasets, it is highly likely that Stable Diffusion has been trained on these images. Additionally,
 456 Bansal et al. [2024] demonstrated successful adaptation towards the style of Van Gogh’s Starry Night
 457 as a single reference image, making this dataset a reasonable interpolation between their successful
 458 results and our more limited findings.

459 Without DP noise or subsampling, we obtained reasonable style transfer results, as shown in Figure 11.
 460 This suggests that style guidance struggles when applied to previously unseen target styles, and that
 461 its effectiveness may depend on prior exposure within the pre-training data.



Figure 10: Sample of paintings by Van Gogh used to generate style guidance embeddings.



Figure 11: Images generated by Stable Diffusion v1.5 with style guidance towards Van Gogh’s *Saint-Paul Asylum, Saint-Rémy* collection using prompts “A painting of Taylor Swift (left) / the Eiffel Tower (center) / a tree (right)”.

462 **D Copyright Protection**

463 Modern generative models typically produce outputs via randomized sampling. Leveraging this
 464 inherent randomness, Vyas et al. [2023] introduced *Near Access-Freeness* (NAF) as a metric to
 465 quantify the similarity between a model’s output and copyrighted content. The key idea is to compare
 466 the output distribution of a potentially infringing model to that of a *safe* model – one trained without
 467 access to the target content.

468 Formally, let *safe* be a mapping from a data point $x \in \mathcal{C}$ (where \mathcal{C} is the collection of copyrighted
 469 samples) to a generative model $\text{safe}(x) \in \mathcal{W}$ that is trained without using x . A canonical example is
 470 the *leave-one-out-safe* model, trained on the full dataset excluding x . Since $\text{safe}(x)$ does not have

471 access to x , the probability that it generates content resembling x is exponentially small. Any such
472 resemblance is considered fortuitous. Formally, the NAF criterion is defined as follows:

473 **Definition 2** (Near Access-Freeness [Vyas et al., 2023]). *Let \mathcal{C} be a set of copyrighted samples and*
474 *\mathcal{W} a set of generative models. Given a mapping $\text{safe} : \mathcal{C} \rightarrow \mathcal{W}$ and a divergence measure Δ , we say*
475 *a model w is k_y -near access-free (or k_y -NAF) on prompt $y \in \mathcal{Y}$ if for every $x \in \mathcal{C}$,*

$$\Delta(p(\cdot|y) \parallel \text{safe}_x(\cdot|y)) \leq k_y.$$

476 If $k_y = 0$, the model is indistinguishable from a safe model, meaning any resemblance to copyrighted
477 material is by random chance. More generally, a small k_y suggests the model is unlikely to generate
478 outputs resembling x with higher probability than a model that has never seen x .

479 D.1 Connection to Differential Privacy

480 NAF is closely related to concepts in *Differential Privacy (DP)* [Elkin-Koren et al., 2023]. Depending
481 on the divergence measure Δ , NAF resembles different DP variants – for example, ε -DP when
482 $\Delta = \Delta_{\max}$ [Dwork et al., 2006], and $(1, \varepsilon)$ -Rényi DP when $\Delta = \Delta_{\text{KL}}$.

483 Translating DP to generative models yields the following definition:

484 **Definition 3** (Differentially Private Generation (DPG)). *Let S and S' be neighboring datasets.*
485 *Denote by $P_S(\cdot|y)$ the distribution over outputs generated by a model trained on, or adapted from, S*
486 *with algorithm \mathcal{A} , where randomness includes both training and generation stages. The generation is*
487 *said to satisfy ε -Differentially Private Generation (ε -DPG) if for every $y \in \mathcal{Y}$,*

$$\Delta(P_S(\cdot|y) \parallel P_{S'}(\cdot|y)) \leq \varepsilon.$$

488 Here, *neighboring datasets* differ by a single data point (or privacy unit). If the training process is
489 ε -DP, then the outputs naturally satisfy ε -DPG via the data processing inequality. One benefit of
490 DPG is the flexibility to add noise during generation rather than training, potentially improving the
491 utility-privacy tradeoff.

492 However, there are notable distinctions. ε -DP offers protection under arbitrary post-processing and
493 multiple outputs, whereas ε -DPG only guarantees privacy for single outputs. Also, under DP, the
494 trained model can be released, but under DPG, only the outputs are safe to share.

495 Elkin-Koren et al. [2023] highlight further differences: NAF is *one-sided*—comparing a model to a
496 fixed safe reference—whereas DPG is *symmetric*. This asymmetry in NAF can enable better utility.
497 Additionally, NAF allows more flexibility in choosing the safe model, which can be exploited in
498 algorithm design.

499 Given these conceptual overlaps, both DP-SGD based training and our proposed private adaptation
500 method DPAgg-TI satisfies ε -DP, so they naturally satisfy ε -NAF with the leave-one-out safe model.

501 We emphasize that this guarantee is meaningful only *within the formal framework of NAF*. It does not
502 imply broader legal immunity or empirical indistinguishability from the original content. However,
503 within this framework, satisfying ε -NAF allows us to argue that any close resemblance between
504 outputs and private training data is no more likely than would be expected from a model that never
505 had access to that data. This theoretical grounding supports the privacy and safety claims of our
506 adaptation method.

507 Importantly, the goal of DPAgg-TI is to adapt to the *style* of a private image set—not its precise
508 content. This distinction matters: style transfer is widely considered to fall under the doctrine of
509 *fair use*, particularly in artistic and creative contexts. As discussed in Elkin-Koren et al. [2023]
510 and further elaborated in legal analysis such as Carlini et al. [2023], generating new content in the
511 style of a work, without reproducing its substantive elements, is generally not considered copyright
512 infringement. Therefore, the use of DPAgg-TI to learn and reproduce stylistic attributes does not
513 contradict the spirit or intent of the NAF framework. Instead, it offers a promising direction for
514 responsibly fine-tuning generative models on private or copyrighted sources while respecting both
515 privacy and intellectual property boundaries.

516 **E Computational Cost Comparisons**

517 Direct comparisons of computational cost across methods are inherently challenging due to differing
 518 training paradigms, optimization procedures, and parameter settings. Nonetheless, to provide a
 519 concrete sense of scale, we report representative computational costs for each method based on
 520 experiments conducted using a Stable Diffusion v1.5 model on a single NVIDIA A100 GPU. Below
 521 we summarize both training and inference overheads (the number of steps are optimized for each
 setup):

Method	Steps	Batch Size	Time	Memory Usage
TI (no DP)	10,000 (for 150 images)	1	25 min	7 GB
		8	2.5 hours	20 GB
TI (DP-SGD)	30,000 (for 150 images)	1	80 min	7 GB
		8	7 hours	20 GB
DPAgg-TI	2,000 per image	N/A	~5 min/image	7 GB
SG	N/A	N/A	N/A	N/A

Table 4: Training cost comparison across methods. Overhead from DP-SGD is relatively modest due to the low-dimensional embedding being optimized. N/A for SG means nothing is trained aside from the base model.

522

Method	Steps	Batch Size	Time	Memory Usage
TI (no DP, DP-SGD, DPAgg-TI)	50	1	1–2 sec	4 GB
	100	1	1–2 min	58 GB
SG (no DP, DPAgg-SG)	500	1	~30 min	17 GB

Table 5: Inference cost comparison across methods.

523 **F Additional Style Transfer and Ablation Results**



Figure 12: Images generated by Stable Diffusion v1.5 using the prompt “A painting of Taylor Swift in the style of <@eveismyname>”, with the embedding <@eveismyname> trained using DPAgg-TI (with different subsample sizes m) and TI with DP-SGD using different values of ε .



Figure 13: Images generated by Stable Diffusion v1.5 using the prompt “An icon of the Eiffel Tower in the style of <Paris 2024 Pictograms>”, with the embedding <Paris 2024 Pictograms> trained using DPAgg-TI (with different subsample sizes m) and TI with DP-SGD using different values of ε .



Figure 14: Images generated by Stable Diffusion v1.5 using the prompt “An icon of a dragon in the style of <Paris 2024 Pictograms>”, with the embedding <Paris 2024 Pictograms> trained using DPAgg-TI (with different subsample sizes m) and TI with DP-SGD using different values of ε .